Lab on a Chip

Cite this: *Lab Chip*, 2012, **12**, 1890

www.rsc.org/loc

PAPER

Quantitative modeling of the behaviour of microfluidic autoregulatory devices

Hyun-Joo Chang,*[a] Wubing Ye[b] and Emil P. Kartalov[ac]

Received 4th October 2011, Accepted 6th March 2012
DOI: 10.1039/c2lc20956j

We develop a theoretical model for a fluidic current source consisting of a via, a detour channel, and a push-up type micro-valve. The model accurately describes the non-linear behaviour of this type of device, which has been previously measured experimentally. We show how various structural parameters and material properties of the device influence the saturated flow rate and the minimum driving pressure required for the device to function as a current source. Conversely, the model can be used to design a fluidic current source with a desired saturated flow rate and low operational pressure. The present model can be straightforwardly applied to microfluidic circuits composed of many functional autoregulatory devices.

Introduction

A multilayer soft lithography technique[1] has enabled a dense integration of micro-valves and pumps within a microfluidic circuit for various applications.[2–4] In general, these device elements consist of shallow microfluidic channels and are characterized by laminar flows due to the low Reynolds number (Re).[5,6] As a result, incompressible Newtonian fluid flow in an axially uniform microfluidic channel can be described by the well-known Poiseuille's law, which states that the flow rate (Q) is proportional to the applied pressure (P) while inversely proportional to the hydraulic resistance (R) of the flow channel.

However, a microfluidic device showing a nonlinear relationship between Q and P is in increasing demand in applications,[7–9] where, for instance, maintaining a constant Q for a wide range of P will be useful.[10–12] For example, in a drug delivery system, a constant flow rate is critical,[13] so pressure fluctuations can be negated with an in-built current source. Yet in reality, obtaining the desired nonlinear behaviour has been a challenge and few studies have been successful. Groisman and co-workers have demonstrated fluidic current source operation by employing a complex winding microfluidic channel along with highly viscous polymer solution as a working fluid.[10] However, practical bio-medical applications need such nonlinear fluidic behaviour to be achieved with water-based biocompatible solutions, which are Newtonian fluids.

Fortunately, autoregulatory devices[11,12,14] offer an elegant and innovative solution to this problem. These devices automatically regulate flow with a combination of a detour channel and a three-dimensional fluidic junction, referred as 'via'.[12,14] Furthermore, the flow behaviour itself is very interesting from the perspective of basic physics, due to multiple features and effects: autoregulatory nonlinear behaviour with Poiseuille flow, saturation,[12] and negative resistance (the "dip").[14]

These devices are also interesting from the perspective of microfluidic engineering as they offer unique capabilities, thereby expanding the toolbox available for microfluidic applications. In particular, point-of-care biomedical diagnostics requires a challenging combination of low cost, flexibility, multiplexing, and portability, while complex function traditionally comes at the expense of complex external control.[15–18] Herein lies the promise of autoregulatory devices, as they offer complex behaviour and function at minimal or no external control, thereby leading to smaller overall size of the diagnostic system.

In this paper, we take another step towards the widespread utilization of autoregulatory devices by providing a theoretical model for their behaviour, which has been confirmed by previous experimental data.[12] This model can be used to predict the flow behaviour as a function of the Young's modulus of the material and of the device's architectural parameters such as length, height, and width of a microfluidic channel.

Specifically, we consider several aspects to reflect on the final modeling. First, we account for the PDMS microchannel swelling with an applied pressure,[19,20] by incorporating Gervais's formula[21] in our calculations. Second, we show that our experimentally confirmed theoretical model[23] for push-down valves can be used for push-up[22] valves as well. Third, we demonstrate that the nonlinear response can be successfully modeled through a combination of Poiseuille's law and the above two aspects. Finally, we show that the resulting model is in good agreement with our experimental data on the current source.

[a]*Dept. of Pathology, Keck School of Medicine, University of Southern California, 2011 Zonal Avenue, Los Angeles, CA 90089-9092, USA. E-mail: hyunjoo@usc.edu*
[b]*Dept. of Mechanical Engineering, California Institute of Technology, 1200 E California Blvd, Pasadena, CA 91125, USA*
[c]*Dept. of Electrical Engineering, California Institute of Technology, Mail Code 200-36, Pasadena, CA 91125, USA. E-mail: kartalov@usc.edu; Fax: +1 323-442-3049; Tel: +1 323-442-3211*

Description of a PDMS autoregulatory device

In Fig. 1, we show a schematic diagram of the fluidic current source, which is used for experimental measurements on pressure-driven flow presented in the previous literature.[12] We develop an analytical model based on these data. A long straight main channel and a detour channel bypassing from the main channel to the micro-valve region are designed. This detour channel is one of the two important integral parts in the current source device; the other important part is a via, which chooses either push-up or push-down configuration for the valve design. The valve membrane thickness, shown in Fig. 1b, is assumed to be 5 μm, which is estimated from the known spin-coating formula.[24] Other structural parameters are dealt with in great detail in our earlier publication.[12]

The PDMS microfluidic device was made of Sylgard 184. The mixing ratio between the base and the curing agent of the Sylgard as well as the curing time and the temperature can control the stiffness of the resulting PDMS, hence the Young's modulus of the PDMS.[25] The rigidity of the material determines valve action and the channel deformation[21] by an internal pressure; therefore our final model should include the effect of the Young's modulus. Further detailed experimental procedures regarding the fabrication and the measurement can be found from our earlier literature.[12]

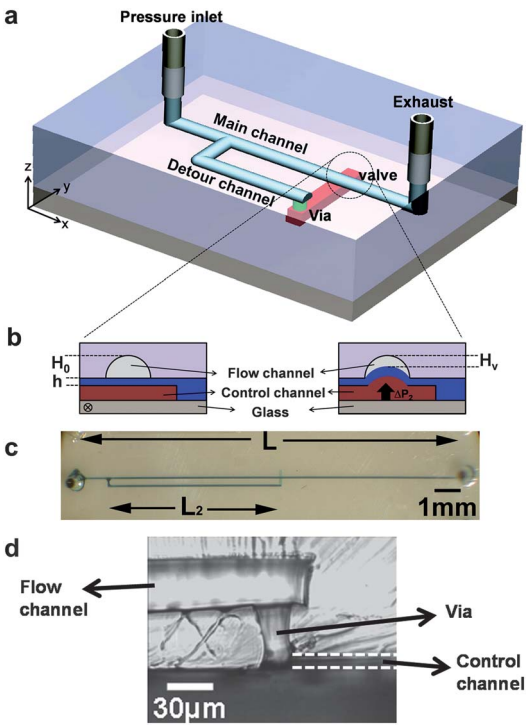

Fig. 1 Microfluidic current source device. (a) The device consists of two PDMS microfluidic layers. The upper one has the main flow channel and the detour channel, while the lower one has the control channel. Both channels are connected through via. (b) Cross-section view of the push-up valve. The valve has the flat membrane geometry whose thickness h is determined by the spin speed. The boundary of the flow channel is round in shape, while the control channel is in rectangular shape. (c and d) Photographs of the scale of the fabricated current source and via (courtesy of *Proc. Natl. Acad. Sci. U. S. A.*, ref. 12, copyright© by the National Academy of Sciences).

Fig. 1d shows an optical microscope image of the 'via', connecting channels on two different levels – the control channel in the lower layer and the flow channel in the upper layer. This via enables propagation of the static pressure at the entrance of the detour channel to the dead-end point, where the micro-valve actuates to control the flow in the main channel. Note that the net upward pressure held across the valve membrane (blue region in Fig. 1b) is equal to the pressure drop in the main channel between the detour entrance and the value region (ΔP_2).

Model for push-up valve

The current source device regulates the flow rate passing through the main channel by means of the push-up valve. Studer and co-workers have performed the three-dimensional finite-element method (FEM) to understand both push-up and push-down valves.[22] The numerical simulation has revealed that the required pressure needed to completely close the channel is 10 times smaller in the case of a push-up valve than a push-down valve with structural dimensions identical to the push-up valve. On the other hand, an experimentally confirmed model has been developed for the push-down case by combining three simpler linear models, a thick beam, a thin spring, and a thick spring model.[23] Here, we extend the regime of the validity to include the push-up case by introducing a scaling factor k, which we refer to as a *membrane geometry factor*. Then, we can write the required 'net' closing pressure measured across the valve membrane as[23]

$$\Delta p_{up}(H_0) = k \cdot E \ln[1 + (16\ H_0^2/3)(w_v^{-2} + l_v^{-2}) + 4H_0(h^3 + 16H_0^2h/3 - 16H_0^3/5)(w_v^{-4} + l_v^{-4})] \quad (1)$$

where E is Young's modulus of the material (ratio of stress to strain), H_0 is the height of the flow channel to be completely closed and w_v, l_v, and h are structural parameters for the geometry of the micro-valve – width, length, and membrane thickness. Though we will try to extract a proper k value through fitting processes with experimental data, we would like to note that k of 0.1 gives the best fit, which is consistent with the previous FEM simulation result.

Theoretical model

Effective channel model

Before developing a model for the realistic autoregulatory device shown in Fig. 1d, we will begin with a rather simple situation as depicted in Fig. 2a. A straight flow channel with length of L ($=L_1 + \Delta + L_2$) has a small bulge or a dimple with length of Δ (assumed to be much smaller than L_1 or L_2). Then, we define the deformation ratio as $\gamma = H_v/H_0$, where H_0 and H_v are the original and the deformed channel height, respectively. It should be noted that the presence of dimple (bulge) depicts a situation where a fluid flows in the forward (reverse) direction (see Fig. 3).

In this section, we will present the concept of the effective channel height, which will be useful to model a flow channel with varying height. As is well known, various useful concepts in the electrical circuit design can be adopted to the case of microfluidics. For example, in the electrical circuit system, the concept

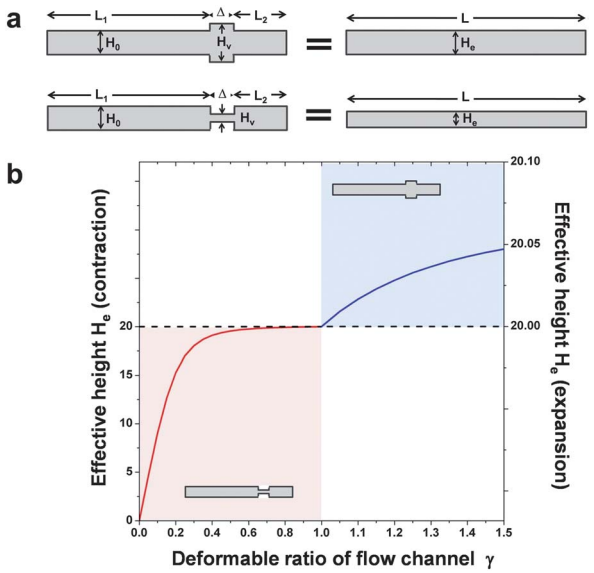

Fig. 2 Effective channel height. (a) Three different channel segments are connected in series: channel 1 (2, 3) has length L_1 (Δ, L_2) and height H_0 (H_v, H_0). The multiple channels can be regarded as a straight channel with a length L ($= L_1 + \Delta + L_2$) and an effective channel height H_e. The length Δ and height H_v of the middle channel are expressed as εL and γH_0, where ε and γ are the proportional constants. (b) When H_0, L, and ε are given by 20 μm, 14.2 mm, and 0.01, respectively, the deformable ratio γ has a strong effect on the effective channel height. For $\gamma > 1$ or $\gamma^3 > \varepsilon$, the effective channel height can be approximated as H_0 (blue box). While, for $\gamma^3 < \varepsilon$, the effective channel is lower than H_0 below γ of ~0.4 (red box).

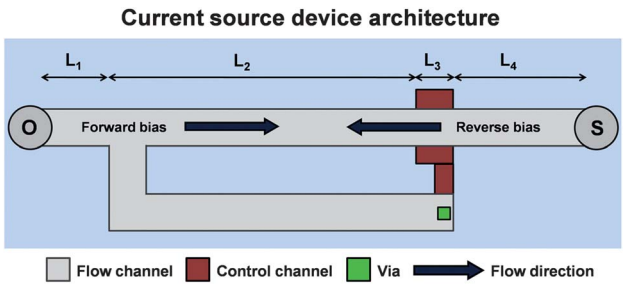

Fig. 3 Top view of the current source architecture. The channel in grey (red) indicates the flow (control) channel in the upper (lower) layer. The flow channel is connected to the control channel by via (green box). The black arrows indicate flow directions. The forward (reverse) bias allows a positive (negative) pressure drop across the detour channel to actuate the push-up valve.

of effective resistance (R_{eff}) has been proved to be very useful when interpreting a composite of resistors. One can always find a certain R_{eff} for any given network of resistors. Then, the overall behaviour of the electrical current is simply given by $I = V/R_{eff}$. On the other hand, in microfluidics, the hydraulic resistance R connects between Q and P through the Poiseuille's law. Then, we can make correspondence between {Q and P} and {current (I) and voltage (V)}, respectively.

Borrowing the concept of effective resistance in electrical circuit analysis, we can define an effective height H_e such that hydraulic resistance of a uniform channel with H_e will result in the same Q for a given P. To derive H_e, we have used the fact that (1) Q is conserved throughout the entire channel and (2) the Poiseuille's law holds within a uniform section of the channel. In Fig. 2b, we plot effective H_e as a function of γ, where we have fixed Δ at a constant $0.01 \times L$. For example, in the case of $\gamma > 1.0$ (bulging), we find that H_e hardly changes. However, in the case of $\gamma < 1.0$ (dimple), H_e abruptly decreases when γ goes below 0.4. This result shows that the fluidic 'bottleneck' is a critical element to govern the overall flow dynamics though it only spans over a very small portion (1%) of the channel. This behaviour in the effective channel height captures the essential aspect of our autoregulatory system and shows how a constant flow rate can be generated. It should be noted that channel heights in the actual device are not such a simple two stepwise but a continuously varying function of space in the form of $H(x)$. Even in such a general situation, we can always define an effective channel height, from which we can define an effective hydraulic resistance.

Poiseuille's law for a rectangular cross-sectional channel

A cross-sectional geometry of a microfluidic channel determines the hydraulic resistance[26] (R). For instance, in the case of a cylindrical cross-section, R is inversely proportional to the fourth power of its radius. In the case of a rectangular cross-section with a height H_0 and width W ($W \gg H_0$), R is inversely proportional to the third power of H_0 and the first power of W. When an actual geometry is slightly deformed from these ideal simple geometries, we can introduce a geometrical correction factor[27] α. The actual geometry of our microfluidic channel is not either a perfect circle or a rectangle but a wedge-like shape with a half-elliptical upper contour and a flat bottom.[1] However, it turns out that taking α to be 1 is legitimate when the aspect ratio H_0/W is very small. Then, we can write R as

$$R = \frac{12\eta L}{H_0^3 W}, \tag{2}$$

therefore the Poiseuille's law is given by:[28]

$$Q = \frac{H_0^3 W}{12\eta L} P. \tag{3}$$

Here, H_0 and W are the height and width of a microfluidic channel. P denotes a pressure drop across the main flow channel with a length of L as shown in Fig. 1a and 3, that is, $P = P(x = 0) - P(x = L)$. η is a dynamic viscosity of a working fluid.

Model for a non-deformable PDMS channel

In this section, we develop a model for a non-deformable PDMS channel. Fig. 3 shows a two-dimensional layout of the main flow channel, the detour channel, the via, and the valve. We conceptually divide the main channel into four different sections with channel lengths of L_1, L_2, L_3, and L_4. We note that flow rates in all sections must be identical (conservation of mass). The total pressure drop across the entire system (from O to S) will be given by the sum of partial pressures in their respective sections such that

$$P = \Delta P_1 + \Delta P_2 + \Delta P_3 + \Delta P_4 = \frac{12\eta(L_1 + L_2)}{H_0^3 W} Q + \frac{12\eta L_3}{H_v^3 W} Q + \frac{12\eta L_4}{H_0^3 W} Q. \quad (4)$$

Note that the above expression for P now includes two unknowns, Q and H_v. Therefore, we need to construct one more equation to solve P as a function of Q.

If we apply eqn (3) to the detour channel since Q remains constant along the channel, we obtain

$$Q = \frac{H_0^3 W}{12\eta L_2} \Delta P_2. \quad (5)$$

Here, ΔP_2 is the pressure drop across L_2, which is also equal to the net pressure held across the valve membrane. From eqn (1), we know how much net pressure is required to completely close the flow channel with the height H_0. In general, however, ΔP_2 is less than $\Delta p_{up}(H_0)$ and the channel height H_v lies between 0 and H_0. Let us find out an expression for ΔP_2 in terms of $\Delta p_{up}(H)$. One plausible candidate is

$$\Delta P_2 = \Delta p_{up}(H_0) - \Delta p_{up}(H_v). \quad (6)$$

The above equation indeed satisfies boundary conditions at the two extreme conditions: If the net pressure is vanishingly small ($\Delta P_2 = 0$), then we obtain a trivial solution of $H_v = H_0$. If the channel is nearly completely closed ($H_v \approx 0$), then the required net pressure to maintain this configuration must be equal to $\Delta p_{up}(H_0)$. With this assumption, we can eliminate ΔP_2 in eqn (5) such that

$$Q = \frac{H_0^3 W}{12\eta L_2} \left[\Delta p_{up}(H_0) - \Delta p_{up}(H_v)\right]. \quad (7)$$

Now we have two unknowns, Q and H_v, and two equations, eqn (4) and (7). Therefore, we can obtain the $P(Q)$ curve or $Q(P)$ curve by numerically solving them; first, one obtains Q as a function of H_v using eqn (7). Then, the right hand side of eqn (4) can be rewritten as a function of H_v, which means $P(H_v)$ is obtained. By comparing $Q(H_v)$ and $P(H_v)$, one can plot either $P(Q)$ or $Q(P)$ and this completes our problem.

Fig. 4a shows the flow rate (Q) as a function of applied pressure P, which clearly shows nonlinear behaviour after a certain threshold value of P. At above this value, Q does not show noticeable change for a large variation in P, which is the required property to function as a fluidic current source. Mathematically, the saturation point is defined as the point at which the slope of the $Q(P)$ curve becomes zero (Fig. 4b). In fact, after a certain threshold value of P, dQ/dP is already very small but approaches true zero very slowly. This behaviour can also be seen from the evolution of H_v as shown in Fig. 4c; H_v seems to saturate at a certain non-zero value but H_v will go down to zero in the limit of large P ($Q(P)$ will go to zero at complete closing of the flow channel. However, in practice, we will see the breakdown of microfluidic channels before reaching this high pressure limit.).

Saturated flow rate and pressure required to reach the saturation

When designing a fluidic current source, there are two important considerations: (1) the pressure needed to reach the saturation point should be minimized and (2) we should be able to control

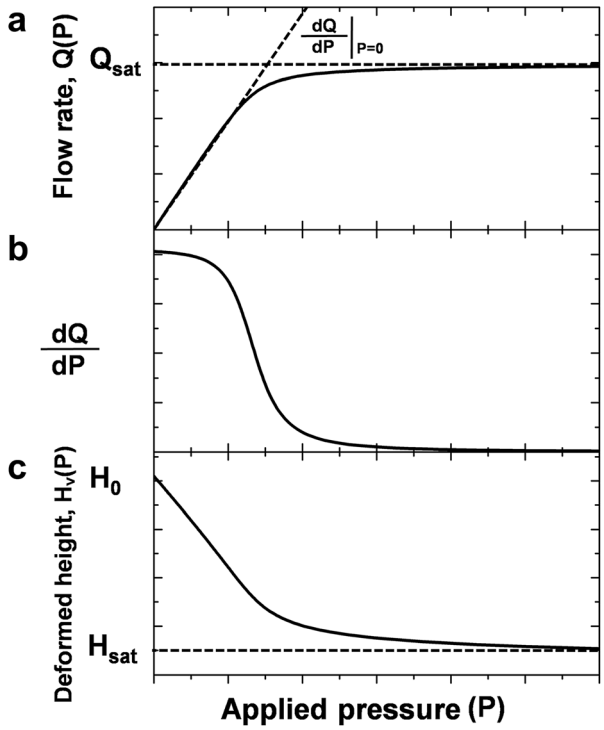

Fig. 4 Characteristics of the current source. (a) The Q–P curve shows the nonlinear behaviour. The flow rate remains constant beyond the saturation pressure. The slope at the initial condition is inversely proportional to the hydraulic resistance from Poiseuille's law. (b) The saturation pressure is defined as a point where the slope of $dQ/dP(P)$ is zero. (c) The partial flow channel height H_v is deformed by the pressure-actuated push-up valve. The $H_v(P)$ curve has the saturation pressure, resulting in the nonlinear hydraulic resistance.

a constant flow rate at the saturation. We will answer these by directly solving eqn (4) and (7), where we assume a perfectly rigid channel that does not suffer from the channel deformation. We also simplify the expression for the needed pressure for complete closing of the valve (eqn (1)) by assuming $h \gg w_v$, l_v such that

$$\Delta p_{up}(H_v) \approx k \cdot E \ln[1 + (16H_v^2/3)(w_v^{-2} + l_v^{-2})] \quad (8)$$

Using the above simplification, we can write $\Delta p_{up}(H_0) - \Delta p_{up}(H_v)$ at the saturation ($H_v \ll H_0$) as

$$\Delta p_{up}(H_0) - \Delta p_{up}(H_v) \overset{H_v \ll H_0}{\rightarrow} k \cdot E \ln\left[1 + \left(16H_0^2/3\right)\left(w_v^{-2} + l_v^{-2}\right)\right] \quad (9)$$

We plug eqn (9) into (7) to obtain the expression for the saturated flow rate in terms of structural parameters.

$$Q_{sat} \approx \frac{H_0^3 W}{12\eta L_2} kE \ln\left[1 + \left(16H_0^2/3\right)\left(w_v^{-2} + l_v^{-2}\right)\right]. \quad (10)$$

On the other hand, the initial slope in the $Q(P)$ curve is given by

$$\left.\frac{dQ}{dP}\right|_{P=0} = \frac{H_0^3 W}{12\eta L}. \quad (11)$$

Note that H_v decreases with a rather steep slope from the beginning as shown in Fig. 4c. However, the effective channel height H_e (Fig. 2b) decreases very slowly because the valve region

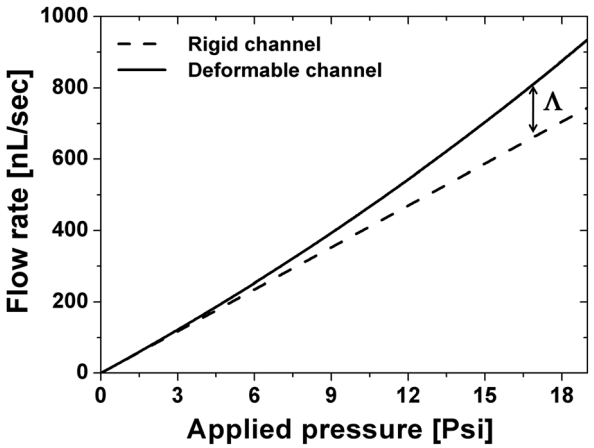

Fig. 5 Response of the Q–P curve. The flow rate increases in the linear fashion in the rigid channel and its slope is inversely proportional to the hydraulic resistance, which is independent of the applied pressure (dashed line). On the other hand, the resistance in the deformable PDMS channel is varied as the applied pressure is increased, leading to the upward curvature of the Q–P curve at a high pressure (solid line).

occupies only a small portion of the entire flow channel. This is the reason why the initial slope of the $Q(P)$ curve does not change too much up to the saturation point. For ideal current source operation, it is important to maximize the initial slope so as to minimize the operational pressure. From eqn (11), we can see that the channel height H_0 seems to be the dominant factor, since the slope depends on the cube of H_0. The same cube dependence can be found from Q_{sat} (eqn (10)). This observation raises a concern whether or not we can control Q_{sat} and the dQ/dP independently, which will be discussed in the Results section.

Model for a deformable PDMS channel

Now we consider the effect of the PDMS deformation due to the internal pressure by the flowing fluid itself. We will use the result developed for a straight PDMS channel in the previous literature.[21] The displacement from the original channel height will be described by a perturbation factor Λ, which is defined as

$$\Lambda(x) = c\frac{P(x)W}{EH_0} \tag{12}$$

and

$$H(x) = H_0 \quad (1 + \Lambda(x)) \tag{13}$$

where c is an unknown proportionality constant and $P(x)$ denotes the internal pressure along the axis of the main flow channel. It should be noted that we will neglect this channel expansion in the transverse direction so that $W(x) = W$, which is legitimate since $W/H_0 \gg 1$. Now we can apply this perturbative approach to find corrections to the unperturbed flow rate in the absence of the channel deformation (the dotted line in Fig. 5). We can solve the reduced Navier–Stokes equation[20,21,26,29] for the above situation to obtain a new velocity profile. The proper surface integration of the velocity profile over the cross-section of the channel gives the corrected flow rate Q, which now includes c and E, properties of the PDMS used.[20,21]

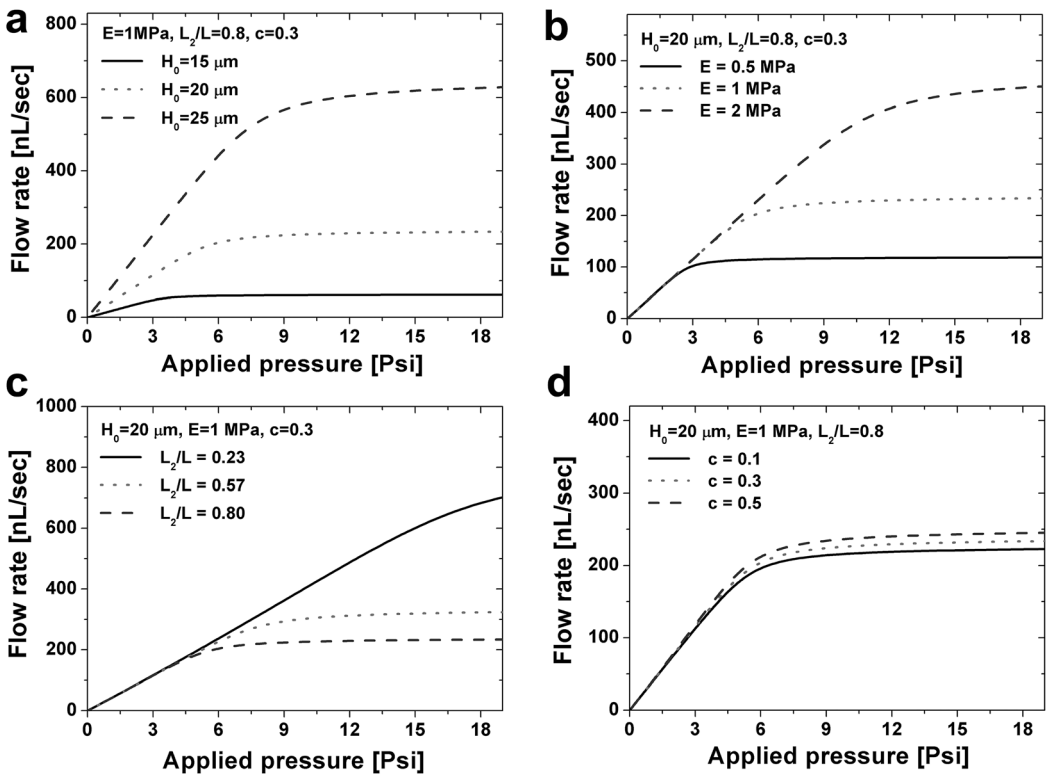

Fig. 6 Simulation of the $Q(P)$ curve for various values of (a) initial height of the flow channel H_0, (b) Young's modulus E, (c) detour ratio L_2/L, and (d) degree of PDMS deformation c. Tuning parameters assumed here are relevant to actual fabricated devices.[12,14,21,25]

$$Q = \frac{H_0^4 E}{48 c\eta L}\left[\left(1 + \frac{cW}{EH_0}P\right)^4 - 1\right] \quad (14)$$

In Fig. 5, we plot the result of eqn (14) along with the rigid Poiseuille's straight channel having the identical dimensions. At our typical working pressure of around 20 psi, errors between the two models can be as high as 20%, which justifies the need for such correction. Thus, eqn (4) has to be changed to

$$P = \frac{EH_0}{cW}\left[\left(1 + \frac{48c\eta(L_1 + L_2)}{H_0^4 E}Q\right)^{1/4} - 1\right] + \frac{12\eta L_3}{H_v^3 W}Q + \frac{EH_0}{cW}\left[\left(1 + \frac{48c\eta L_4}{H_0^4 E}Q\right)^{1/4} - 1\right], \quad (15)$$

where the applied pressure P is expressed as a function of H_v. We neglect this bulging effect for the valve region, since L_3 is just about 0.7% of the total length ($= L_1 + L_2 + L_3 + L_4$).

Following similar steps in eqn (5)–(7), we obtain the expression for the flow rate Q as a function of H_v.

$$Q = \frac{H_0^4 E}{48 c\eta L_2}\left[\left\{1 + \frac{cW}{EH_0}\left(\Delta p_{up}(H_0) - \Delta p_{up}(H_v)\right)\right\}^4 - 1\right]. \quad (16)$$

Therefore, comparing $P(H_v)$ [eqn (15)] and $Q(H_v)$ [eqn (16)], one can plot Q as a function of P.

Results

In Fig. 6, we plot various $Q(P)$ curves as we vary various parameters. First let us look at results in Fig. 6a. We vary H_0 while fixing other parameters. As expected, as dQ/dP increases Q_{sat} increases accordingly. To get a rather independent control of Q_{sat} over dQ/dP, we note that the expression for Q_{sat} [eqn (10)] contains additional parameters, E and L_2, which are not included in dQ/dP [eqn (11)]. The evolution of Q_{sat} as a function of E and L_2 is presented in Fig. 6b and c, respectively. Within a reasonable range in E for PDMS, we can control Q_{sat} in the range of 100 nL s^{-1} to 400 nL s^{-1}. However, E is a quantity fixed during the fabrication step. Therefore, to allow variations in Q_{sat} within the same PDMS microfluidic chip, we must control L_2. Fig. 6c shows this result: Q_{sat} is inversely proportional to L_2. This result shows that the detour channel is an essential part of our autoregulatory system. Finally, we also investigate the effect of PDMS bulging shown in Fig. 5. We vary a constant that controls the degree of the bulging; as expected, only a small variation in Q_{sat} could be obtained.

Now we are in a good position to apply our findings to the experimental data. As noted in the above, the slope is a very sensitive function of H_0. Therefore, we first try to obtain the most reasonable value for H_0 while W, L, and h are fixed to some known values. In fact, when we apply pressure to the port S (reverse bias), the effect of the valve region can be neglected as proven by the effective channel height argument. As we decrease L_2 (or the detour ratio L_2/L), this assumption holds true more and more perfectly. Fig. 7 compares experimental data from our previous work[12] (dots) and a theoretical curve (solid line). Here, we try to fit the curve to the measurement data with $L_2/L = 0.23$. We find that the best fitted curve can be obtained with $E/c = 4.14$ MPa.

Then, we try to fit data obtained from the forward bias experiments (see Fig. 8). In this fitting, E and c are fitting parameters with a constraint of $E/c = 4.14$ MPa. This means only one fitting parameter is used to get good fitted results as shown in Fig. 8. The best fitted results are obtained with $E = 1.2$ MPa and $c = 0.29$, both are within reasonable ranges.

Discussion and conclusions

We develop a theoretical model that can explain how the flow rate changes as we regulate the flow by employing the detour channel. The theoretical model predicts on how the flow rate changes as a function of applied pressure – the $Q(P)$ curve, which

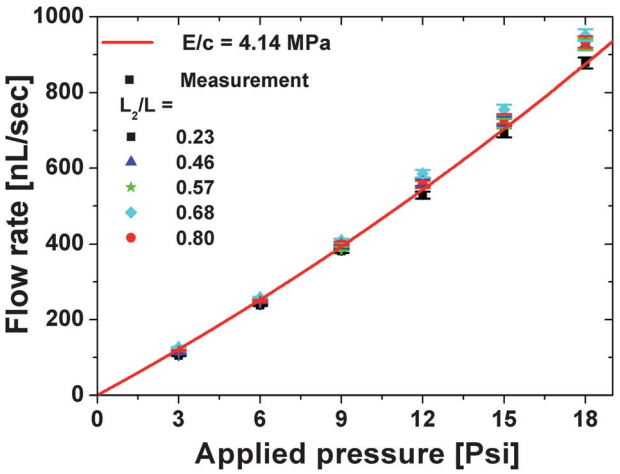

Fig. 7 Comparison of measurement and modeling data in reverse bias. Flow rates are measured as a function of applied pressure given at different detour channel ratios L_2/L (black squares, blue triangles, green stars, blue diamonds and red filled circles). The fit of eqn (14) clearly shows a slightly upward slope (red solid line). The fit parameter E/c of 4.14 MPa is good agreement with measured data.

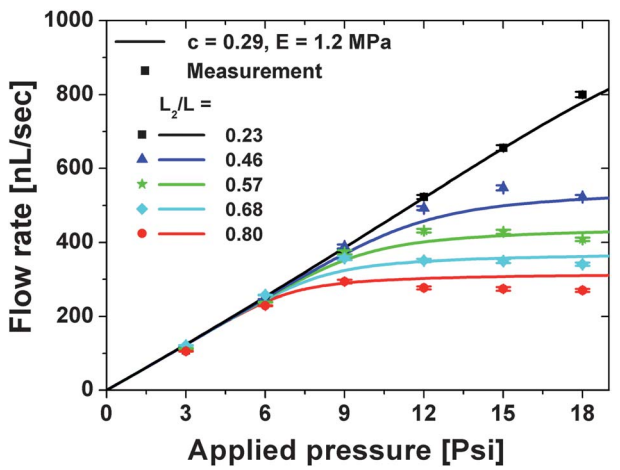

Fig. 8 Comparison of measurement and modeling data in forward bias. From eqn (14) and (15), the nonlinear fit curves (solid lines) are in good agreement with measured data (black squares, blue triangles, green stars, blue diamonds and red filled circles) where fit parameters c and E are 0.29 and 1.2 MPa, respectively. The saturation pressure and flow rate decrease as the detour channel ratio increases.

shows good agreement with the experimental data, though the model is based on a rather simple Poiseuille's law for incompressible, Newtonian fluids. Specifically, we verify that modeling parameters such as (1) flow channel height H_0, (2) Young's modulus of PDMS E, (3) detour channel ratio L_2/L, and (4) membrane geometry factor k have strong influence on the saturation pressure and the saturated flow rate. We also consider the expansion of microfluidic channel height, originated from the softness of PDMS, which would be of more significant concern at a higher pressure.

The autoregulatory effect depends on the ratio of lengths of the "main channel" and "detour channel", rather than the lengths themselves.[12,14] Therefore, the size of such a current source unit is not limited by the length of the constituent channels. However, the device operation is dependent on the proper functioning of the valve, which has geometric limitations[14] and thus limits the size of the unit to ~0.25 mm^2 by current technology. Still, such size allows device densities of over 2500 per inch^2, which is very generous for most conceivable applications. The theoretical model presented here is a building block for the theory of such circuits, just as a single current source is a building block for their physical structure.

Microfluidic devices based on biocompatible fluids will be likely to be useful for a broad range of applications from basic biochemical studies on-a-chip to biomedical fields. Furthermore, it has been argued that further miniaturization of the microfluidic chip size has been hampered by a number of external ports (also known as Medusa) which are indispensable for controlled actuation of micro-valves.[29] The via structure that connects the detour flow channel to the push-up valve allows three-dimensional systematic integration of microfluidic circuit elements, which would help to increase the number density of fluidic components and to enable ultimate device miniaturization. Therefore, we can expect huge reduction in the number of external ports by employing our autoregulatory systems based on these vias. In this context, our modeling will provide useful guidelines to the design of such devices as well as to understand physics behind their behaviour and operation.

Acknowledgements

This work was supported by National Institutes of Health grant 4R00EB007151.

Notes and references

1 M. Unger, H. P. Chou, T. Thorsen, A. Scherer and S. R. Quake, *Science*, 2000, **288**, 113.
2 F. K. Balagadde, L. You, C. L. Hansen, F. H. Arnold and S. R. Quake, *Science*, 2005, **309**, 137.
3 J. W. Hong, V. Studer, G. Hang, W. F. Anderson and S. R. Quake, *Nat. Biotechnol.*, 2004, **22**, 435.
4 A. Y. Fu, H. Chou, C. Spence, F. H. Arnold and S. R. Quake, *Anal. Chem.*, 2002, **74**, 2451.
5 J. P. Brody, P. Yager, R. E. Goldstein and R. H. Austin, *Biophys. J.*, 1996, **71**, 3430.
6 T. M. Squires and S. R. Quake, *Rev. Mod. Phys.*, 2005, **77**, 977.
7 M. Prakash and N. Gershenfeld, *Science*, 2007, **315**, 832.
8 C. Huang, M. Z. Bazant and T. Thorsen, *Lab Chip*, 2010, **10**, 80.
9 F. Lin, W. Saadi, S. W. Rhee, S. Wang, S. Mittal and N. L. Jeon, *Lab Chip*, 2004, **4**, 164.
10 A. Groisman, M. Enzelberger and S. R. Quake, *Science*, 2003, **300**, 955.
11 I. Doh and Y. Cho, *Lab Chip*, 2009, **9**, 2070.
12 E. P. Kartalov, C. Walker, C. R. Taylor, W. F. Anderson and A. Scherer, *Proc. Natl. Acad. Sci. U. S. A.*, 2006, **103**, 12280.
13 B. Ziaie, A. Baldi, M. Lei, Y. Gu and R. A. Siegel, *Adv. Drug Delivery Rev.*, 2004, **56**, 145.
14 J. Liu, Y. Chen, C. R. Taylor, A. Scherer and E. P. Kartalov, *J. Appl. Phys.*, 2009, **106**, 114311.
15 P. Yager, T. Edwards, E. Fu, K. Helton, K. Nelson, M. R. Tam and B. H. Weigl, *Nature*, 2006, **442**, 412.
16 F. B. Myers and L. P. Lee, *Lab Chip*, 2008, **8**, 2015.
17 E. P. Kartalov, J. F. Zhong, A. Scherer, S. R. Quake, C. R. Taylor and W. F. Anderson, *BioTechniques*, 2006, **40**, 85.
18 R. Sista, Z. Hua, P. Thwar, A. Sudarsan, V. Srinivasan, A. Eckhardt, M. Pollack and V. Pamula, *Lab Chip*, 2008, **8**, 2091.
19 S. M. Sirard, P. F. Green and K. P. Johnston, *J. Phys. Chem. B*, 2001, **105**, 766.
20 B. S. Hardy, K. Uechi, J. Zhen and H. P. Kavehpour, *Lab Chip*, 2009, **9**, 935.
21 T. Gervais, J. El-Ali, A. Gunther and K. F. Jensen, *Lab Chip*, 2006, **6**, 500.
22 V. Studer, G. Hang, A. Pandolfi, M. Ortiz, W. F. Anderson and S. R. Quake, *J. Appl. Phys.*, 2004, **95**, 393.
23 E. P. Kartalov, A. Scherer, S. R. Quake, C. R. Taylor and W. F. Anderson, *J. Appl. Phys.*, 2007, **101**, 064505.
24 K. Norrman, A. Ghanbari-Siahkali and N. B. Larsen, *Annu. Rep. Prog. Chem., Sect. C: Phys. Chem.*, 2005, **101**, 174.
25 D. Armani, C. Liu and N. Aluru, *Proceedings of IEEE Micro Electro Mechanical System (MEMS)*, 1999, 222.
26 H. Bruus, *Theoretical Microfluidics*, Oxford University Press, USA, 2007.
27 N. A. Mortensen, F. Okkels and H. Bruus, *Phys. Rev. E: Stat., Nonlinear, Soft Matter Phys.*, 2005, **71**, 057301.
28 J. Happel and H. Brenner, *Low Reynolds Number Hydrodynamics*, Prentice Hall, New York, 1965, p. 34.
29 S. Vyawahare, S. Sitaula, S. Martin, D. Adalian and A. Scherer, *Lab Chip*, 2008, **8**, 1530.